EPJ Web of Conferences **32**, 02017 (2012)
DOI: 10.1051/epjconf/20123202017

ECH and ECCD effects on NTMs stabilization by ECRF in JT-60SA tokamak

C. Sozzi[1], T. Bolzonella[2], D. Farina[1], L. Figini[1], M. Furukawa[4], G.Giruzzi[3], S. Ide, A. Isayama, G. Matsunaga, S. Moriyama, S. Nowak[1] and JT-60SA Research Plan contributors and JT-60SA Team

Japan Atomic Energy Agency, Mukouyama, Naka City, Ibaraki, 311-0193 Japan
[1] Istituto di Fisica del Plasma CNR, Euratom Association, 20125 Milano, Italy
[2]Associazione EURATOM-ENEA, Consorzio RFX, 35127 Padova, Italy
[3]CEA, IRFM, 13108 Saint-Paul-lez-Durance, France
[4]Graduate School of Frontier Sciences, University of Tokyo, Kashiwa 277-8561, Japan

Abstract. The current drive efficiency of the dual frequency (110 GHz and 138 GHz) ECRF system of JT-60SA is studied. The requirements for neoclassical tearing modes (NTMs) instabilities control by ECRF during the initial research phase when only part of the full system will be available are discussed.

1 Introduction

JT-60SA is the large fully superconducting tokamak being built under the Broader Approach Satellite Tokamak Programme jointly by Europe and Japan, and under the Japanese national program to support the ITER programme and DEMO design phase [1]. In the framework of the EU and JA combined work on the Research Plan revision [2] of JT-60SA the capability to well localize heating and current drive has been considered for various physics studies, such as the neoclassical tearing modes (NTMs) instabilities control, key issue to sustain high beta plasmas in fusion devices. In the initial research phase 3 MW of ECRF at 110 GHz and 1.5 MW at 138 GHz will be available out of the 7 MW foreseen for later phases [3]. The maximum available power from the NBI system in the initial Research Phase is $P_{NNBI}+P_{PNBI}$=10+10 MW in Hydrogen and 10+20 MW in Deuterium [2]

An extensive analysis of ECH and ECCD characteristics have been performed for standard (#2, Bt~2.25 T, I_p=5.5, q95~3, n_e/n_{GW}=0.5, β_N=3.1) and advanced (#5, Bt~1.72 T, I_p=2.3, q95~5.8, n_e/n_{GW}=0.85, β_N=4.3) operational scenarios described in the Research Plan [2]. . Absorption of EC waves at second extraordinary harmonics (X2) with the EC beams entering the plasma from the low field at about half height of the poloidal section above the mid-plane has been considered. The EC power and driven current densities have been calculated in a simplified launching geometry by using the GRAY beam tracing code [4] for a wide range of toroidal (±20°, being ±15° the range foreseen with the present antenna design [5]) and poloidal (-20° to +40°) injection angles.

This paper is organized as follows. In section 2 the ECRF beam produced by the antenna system is briefly described. In section 3 the current drive efficiencies obtained with beam tracing calculation for the two frequencies are presented. Section 4 deals with the study of NTMs stabilization in scenarios 2 and 5. Finally section 5 reports a summary of the main findings and caveat.

2 ECRF beams modelling

The reference design for the ECRF antenna has been described in [5, 6]. For each beam the antenna is composed of two mirrors (see Figure 1). The first one is a flat mirror positioned in front of the tip of the 60.3 mm corrugated waveguide. This first mirror reflects the beam towards a wide, fixed cylindrical mirror. The flat mirror can be moved along an axis parallel to the waveguide in such a way that the impact point of the beam on the cylindrical mirror and the actual angle of reflection towards the plasma seen by the beam is also changed, scanning as a consequence the poloidal angle of injection. The size and the curvature of the cylindrical beam has been optimized in order to obtain the required poloidal angular range.

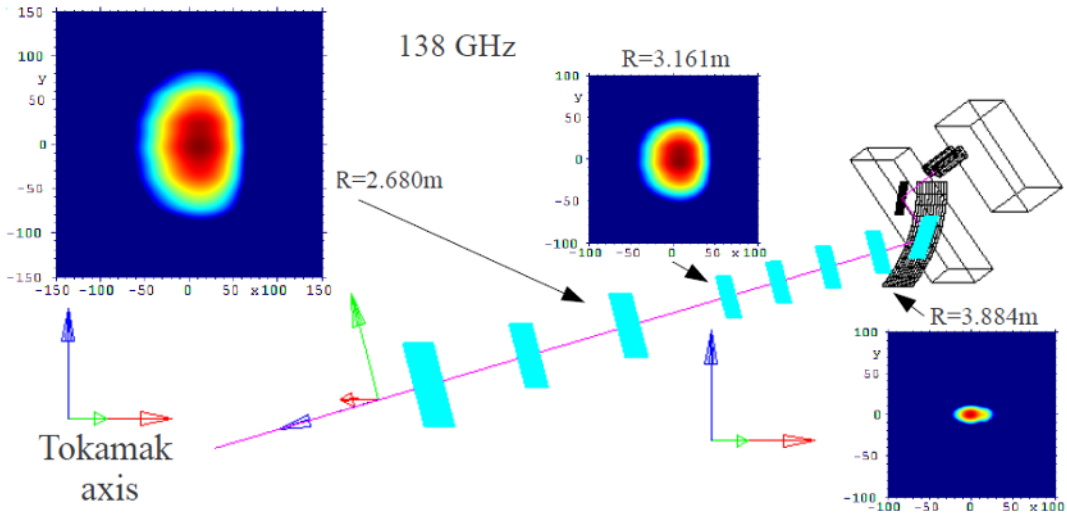

Fig. 1. Layout of the ECRF antenna with the $1/e^2$ (power) pattern of the resulting beam at 138 GHz, in the locations indicated by the black arrows. Axis x(red), y(green) in the beam patterns are oriented as shown in the cartesian coordinate system. Blue axis (z coordinate) is also parallel to the wave vector.

This layout has been modelled using a Physics Optics numerical tool [7, 8] which computes the field distribution in vacuum resulting from the superposition of the primary sources as the HE_{11} mode propagating in the waveguide and of the resulting currents induced on the reflecting surfaces.

The purpose of the modelling was to obtain a handy Gaussian beam approximation to be used as an input for beam tracing calculation at both the frequencies of 110 and 138 GHz, also keeping into account the astigmatism of the beam. After the secondary reflection the beam is in fact rather astigmatic along the poloidal direction, as can be observed in Figure 1 and pointed out in [6] for 110 GHz. The beam has then been fitted using astigmatic Gaussian beam representation in the relevant part of the path of propagation, i.e. after the cylindrical mirror. For perpendicular injection, i.e. with wave vector having nil toroidal components, x axis is coincident with the toroidal direction and y axis with the poloidal one. The beam waist for such direction is located in the plasma at R=3.884m corresponding to the region ρ_t=0.8-0.9. The major radius of the plasma axis is R=2.96m and the centre of the cylindrical mirror is located at R=4.125m.

The parameters of the fitted Gaussian beams, used for the beam tracing calculations are reported in Table 1. The beam propagation obtained with Physics Optics calculation is fairly accurate keeping into account diffraction effects and aberrations. However, some approximations have been introduced in order to simplify the beam tracing computations. In scanning the steering range, the launching point has been kept fixed. The layout of the antenna imply instead that at different injection angles different launching point correspond and that the astigmatism of the beam is a function of the

poloidal injection angle, as shown in [6]. The Gaussian approximation here used is strictly valid for beam launch towards the plasma centre and holds as a representative average behaviour for other cases. Moreover, the elliptical footprint of the launched beam is slightly rotating for non zero toroidal injection angles. This last effect is in comparison of second order if not negligible.

Table 1. Parameters of the astigmatic Gaussian beams. Left to right: frequency, beam waist size in y and x, their distances from the cylindrical mirror centre (>0 towards plasma) and the coordinates of the launching point, measured in the reference frame of the tokamak axis (plane y=0 contains the cylindrical mirror centre).

Frequency [GHz]	w_{0y} [m]	w_{0y} [m]	dw_{0y} [m]	dw_{0x} [m]	x ≡ R [m]	y [m]	z [m]
110	0.013	0.018	0.275	-0.105	4.125	0.060	0.822
138	0.010	0.018	0.255	-0.125			

3 Current drive efficiencies in Scenario 2 and Scenario 5

Magnetic equilibria, temperature and density profiles [1] used as input of GRAY code are shown in figure 2.

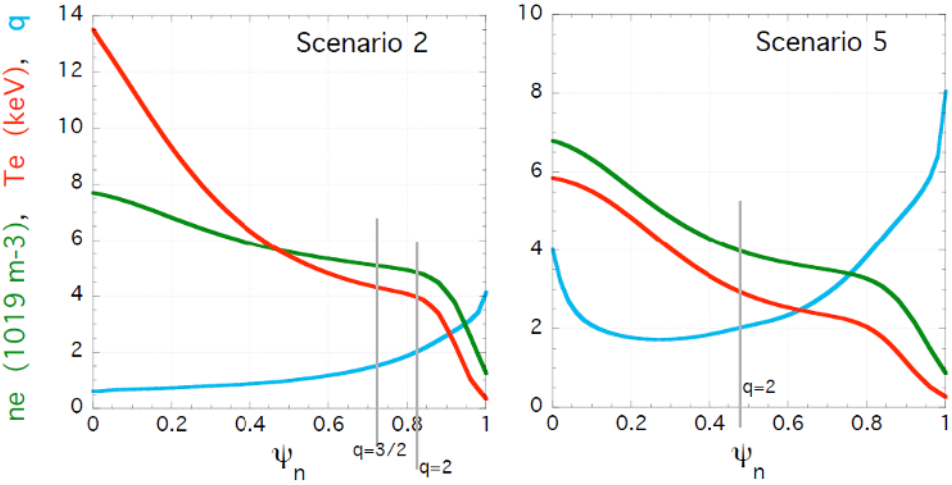

Fig. 2. Density, electron temperature and safety factor profiles for the two scenarios under investigation.

GRAY performs the computation of the Quasi Optical propagation, the power absorption and driven current of an astigmatic Gaussian beam of EC waves in a general tokamak equilibrium, taking into account trapped particle effects and the full wave polarization. The absorption coefficient is computed solving either the fully or weakly relativistic dispersion relation [9]. The EC current driven is computed taking into account momentum conservation [10].

The analysis has shown that for 110 GHz the cold resonance surface of the second harmonic EC wave is located at about R = 3.38 m for Bt = 2.25 T (corresponding to operating scenarios 1,2,3), which is fairly off-axis region. Furthermore, the EC wave will be fully absorbed before reaching this surface due to the Doppler shift effect. At this field of operation EC waves can only penetrate up to ρ~0.8 and have therefore limited applicability. For 138 GHz frequency the 2nd harmonic absorption layer for scenario 5 (1.72 T) is located in the high field side with respect to the magnetic axis, but the penetration of EC waves is prevented by the third harmonic layer on the low field side or in the core, depending on plasma temperature and density. In this case the 2nd harmonics layer in the high field

side can not be effectively used, while core electron heating schemes using 3rd harmonics would be possible.

The current drive efficiencies computed across the steering range are plotted in figure 3 for scenarios 2 (at 138 GHz, left) and 5 (at 110 GHz, right), which contains two contour plot scales. Black contours represent radius ρ (square root of the normalized toroidal flux) in the (α, β) plane where the deposition occurs. The contour plots in color code represent the driven current in units of kA per injected MW averaged on the deposition region [11]. The poloidal angle is defined by $\tan(\alpha)=N_Z/N_R$ and the toroidal by $\sin(\beta)=N_\phi$, being **N** the refractive index vector.

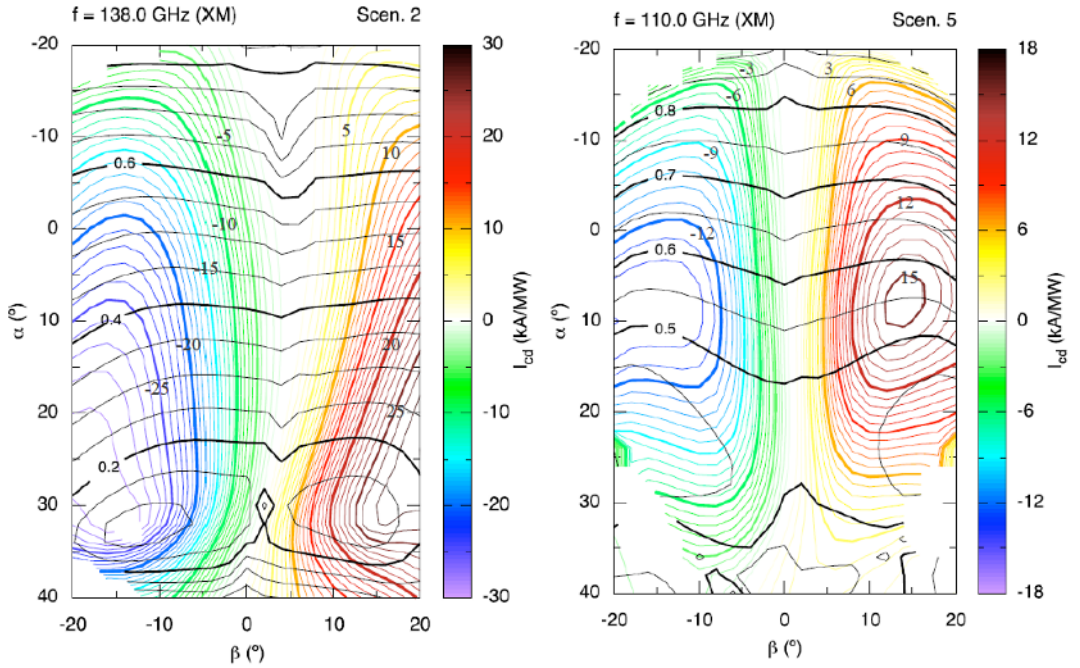

Fig. 3. Contour plots of the current drive efficiency as a function of the steering angles (see text above).

4 Stabilization of NTMs (2,1) and (3,2)

Table 2 below reports in columns 2-9 the local parameters for the three cases of instability studied in this paper with the Generalized Rutherford Equation (GRE). Inspection of figure 3 shows the range of the expected EC current driven in the region where the instabilities are located (see column 10). In column 11 the full e^{-2} current density width of the driven current channel δ_{cd} computed with GRAY is listed.

Table 2. Local parameters used in the GRE.

Scenario	m/n	ρ_t	$L_q=q/q'$ [m]	$L_p=nT/(\partial(nT)/\partial r)$ [m]	β_p	n_e [$10^{19}m^{-3}$]	T_e [keV]	I_P [MA]	I_{cd} [kA/MW]	δ_{cd} [cm]
2	2/1	0.79	0.3	0.5	0.37	4.85	4	4.1	1÷6	4÷11
2	3/2	0.7	0.38	0.78	0.38	5.1	4.3	3.84	3÷10	4÷9
5	2/1	0.5	0.63	0.63	1.1	4	2.9	1.36	8÷15	4÷13

The stabilization criterion applied is to reduce the mode at its marginal width w_d through the balance of the EC current drive term and all other terms in the GRE [12]. The stabilizing P_{EC} power

required for NTMs control as a function of the current drive efficiency in the two investigated scenarios is shown respectively in figures 4 and 5.

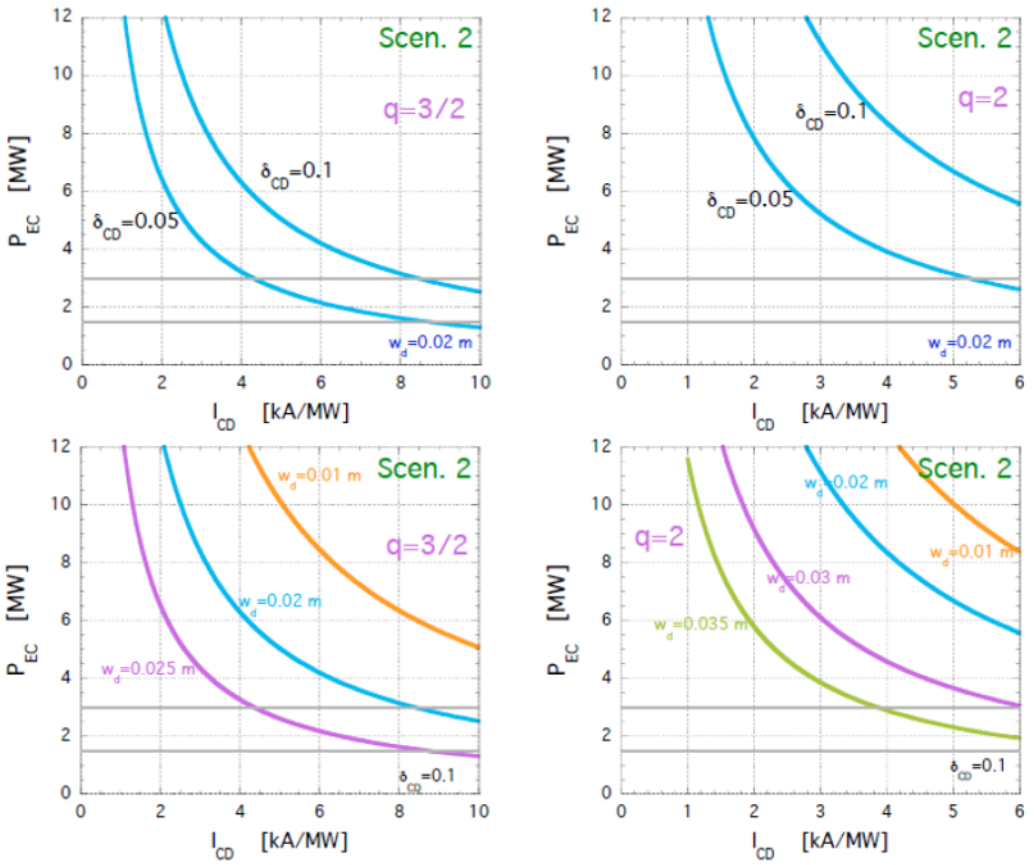

Fig. 4. Stabilizing EC power at 137.6 GHz versus current drive efficiency in Scenario 2 for different cases.

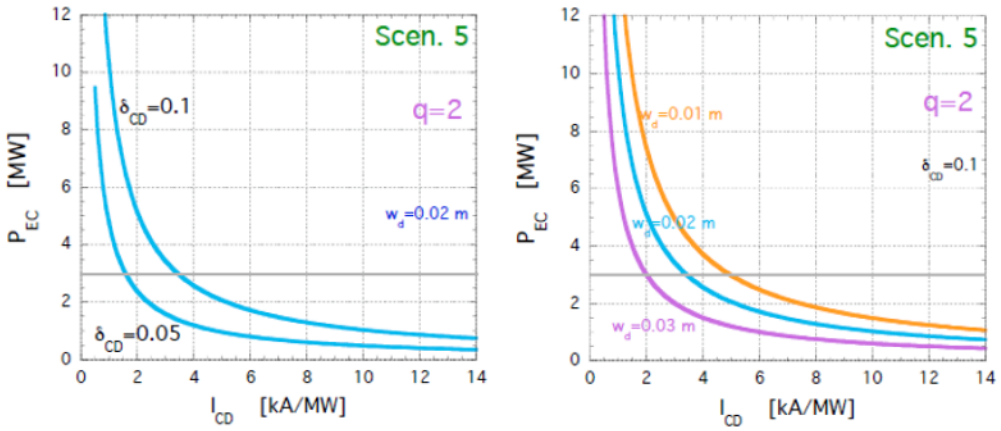

Fig. 5. Stabilizing EC power at 110GHz versus current drive efficiency in Scenario 5

Two representative values of the δ_{cd} parameter (0.05m and 0.1m) have been chosen to show the role of the EC driven current width. Moreover, stabilization thresholds calculated using a range of assumptions for the island width w_d are plotted. This width indicates a stabilizing effect due to the finite perpendicular transport for the incomplete pressure flattening at the island. The reference value here is w_d=0.02m in agreement with typical ranges considered in JET discharges [13]. Generally, margins for stabilization increase at larger w_d and smaller δ_{cd}. The horizontal grey lines at 1.5 and 3 MW indicate the available EC power during the initial research phase.

5 Conclusions

In summary, to overcome limitations of 110 GHz ECRF frequency in Scenario 2 also 138 GHz has been considered. At 2.25 T, 138 GHz can accomplish all the functions: central heating, off-axis CD, NTM control, provided that the CD efficiencies are sufficient for the available power. The same holds for 110 GHz at 1.72 T, where however central heating is generally less efficient.

Those considerations eventually suggested the development of dual frequency gyrotrons at 110 GHz and 138 GHz. The combination of those two frequencies allows fairly good flexibility in all the scenarios.

The power of 3MW of ECRF seems sufficient for stabilization of NTM(2,1) in scenario 5 (at 110 GHz) and NTM(3,2) in scenario 2 (at 138 GHz) for δ_{cd}=0.1m. The same power is marginal for NTM(2/1) in scenario 2, due to the lower current drive efficiency.

A power of 1.5MW of ECRF at 138 GHz could be enough for stabilization of NTM (3,2) in scenario 2 if the marginal width $w_d > 0.025$ m

Enhanced current drive efficiency is found for $15° < \beta < 20°$ in scenario 2, suggesting the extension of the steering range in this region.

Acknowledgments

This work was supported by EURATOM and carried out within the framework of the European Fusion Development Agreement. The views and opinions expressed herein do not necessarily reflect those of the European Commission.

References

1. Y. Kamada et al., Nucl. Fusion **51**, 073011 (2011)
2. Ja Team and EU Team, JT-60SA Research Plan, Version 3, December 2011, http://www.jt60sa.org/pdfs/JT-60SA_Res_Plan.pdf
3. A. Isayama et al., Pl. Fus. Res. **7**, 2405029 , (2012)
4. D. Farina, Fus. Sci. Techn. **52**, 154 (2007)
5. T. Kobayashi et al., Fus. Eng. Des. **86**, 763 (2011)
6. T. Kobayashi et al., Fus. Eng. Des. **84,** 1063 (2009)
7. K. Pontoppidan, GRASP© Technical Description, TICRA, Denmark 2005.
8. P. Platania et al, Fus. Sci. Techn. **53**, 77 (2008)
9. D. Farina, Fus. Sci. Techn. **53**, 130 (2008)
10. N.B. Marushchenko et al, Fusion Sci. Techn. **55** 180 , (2009)
11. D. Farina et al., Nucl. Fusion **52,** 033005 (2012)
12. E. Lazzaro and S. Nowak, Plasma Phys. Contr. Fusion **51**, 035005 (2009) and references therein.
13. O. Sauter et al., Plasma Phys. Control. Fusion **44**, 1999 (2002)